Effect of Electron-Withdrawing Fluorine and Cyano Substituents on Photovoltaic Properties of Two-Dimensional Quinoxaline-Based Polymers

Seok Woo Lee
Pukyong National University
MD Waseem Hussain
Hanyang University
Sanchari Shome
Hanyang University
Su Ryong Ha
Hanyang University
Jae Taek Oh
Hanyang University
Dong Ryeol Whang
Hannam University
Yunseul Kim
Gwangju Institute of Science and Technology
Dong-Yu Kim
Gwangju Institute of Science and Technology
Hyosung Choi (hschoi202@hanyang.ac.kr)
Hanyang University
Dong Wook Chang
Pukyong National University

Research Article

Keywords: Electron withdrawing, Fluorine, Cyano substituent, Quinoxaline, Polymer solar cells

Posted Date: October 13th, 2021

DOI: https://doi.org/10.21203/rs.3.rs-957213/v1

Version of Record: A version of this preprint was published at Scientific Reports on December 1st, 2021. See the published version at https://doi.org/10.1038/s41598-021-03763-1.

Abstract

In this study, strong electron-withdrawing fluorine (F) and cyano (CN) substituents are selectively incorporated into the quinoxaline unit of two-dimensional (2D) D–A-type polymers to investigate their effects on the photovoltaic properties of the polymers. To construct the 2D polymeric structure, electron-donating benzodithiophene and methoxy-substituted triphenylamine are directly linked to the horizontal and vertical directions of the quinoxaline acceptor, respectively. After analyzing the structural, optical, and electrochemical properties of the resultant F- and CN-substituted polymers, labeled as PBCl-MTQF and PBCl-MTQCN, respectively, inverted-type polymer solar cells with a non-fullerene Y6 acceptor are fabricated to investigate the photovoltaic performances of the polymers. It is discovered that the maximum power conversion efficiency of PBCl-MTQF is 7.48%, whereas that of PBCl-MTQCN is limited to 3.10%. This significantly reduced PCE of the device based on PBCl-MTQCN is ascribed to the formation of irregular, large aggregates in the active layer, which can readily aggravate the charge recombination and charge transport kinetics of the device. Therefore, the photovoltaic performance of 2D quinoxaline-based D–A-type polymers is significantly affected by the type of electron-withdrawing substituent.

Highlights

- Two-dimensional D–A type quinoxaline-based polymers were designed and synthesized
- Strong electron-withdrawing fluorine and cyano moieties were selectively incorporated into the quinoxaline acceptor in the target polymers.
- The maximum PCE of the device based on fluorinated PBCl-MTQF is 7.48%, whereas that of the device based on cyano-substituted PBCl-MTQCN is limited to 3.10%.

Introduction

The unique advantages of polymer solar cells (PSCs) such as semi-transparent, flexible, light weight, and feasible for scalable roll-to-roll processes render them attractive as a promising green and renewable energy resource [1–3]. In a typical PSC, an *n*-type acceptor and *p*-type polymeric donor form a bulk heterojunction (BHJ) network with large interfacial areas to facilitate charge separation and charge transport [4]. Although fullerene derivatives are the most widely used *n*-type acceptors in recent decades, recent breakthroughs pertaining to non-fullerene acceptors (NFAs) have rapidly changed the paradigm. Compared with fullerene-type counterparts, NFAs possess more effective features such as a tunable electronic structure, broad light absorption, and good morphology for improving device performance [5–7]. Hence, the power conversion efficiency (PCE) of state-of-the-art NFA-based PSCs has exceeded 18% [8].

In addition to the significant progress in *n*-type acceptors, the development of *p*-type polymeric donors with appropriate energy levels, good carrier mobility, and favorable morphologies for realizing high-performance PSCs has been emphasized [9]. These polymers typically comprise alternating electron-donating (D) and electron-accepting (A) units along the polymer chain, in which a useful intramolecular

charge transfer (ICT) state is readily generated. Among the various promising building blocks for D–A type polymers, the quinoxaline moiety has emerged as a promising “A” component because of its unique merits, such as simple synthetic routes and facile structural variations [10]. Additionally, its mild electron-accepting ability facilitates the preparation of medium-bandgap polymers. The combination of medium-bandgap polymeric donors and narrow-bandgap NFAs allows BHJ photoactive layers to exhibit beneficial complementary light absorption profiles [11]. Moreover, it was recently discovered that the incorporation of strong electron-withdrawing substituents into D and/or A units can efficiently improve the photovoltaic performance of the corresponding D–A-type polymers [12–14]. In this regard, several quinoxaline-based D–A-type polymers possessing electron-withdrawing substituents have been investigated to achieve high-performance nonfullerene PSCs [15–18]. However, more systematic studies associated with this interesting topic are still required because the effects of the electron-withdrawing substituents on the photovoltaic properties of the polymers are highly susceptible to the chemical composition and configuration of the polymer structure.

In this study, two-dimensional D-A type polymers with strong electron-withdrawing fluorine (F) atoms or cyano (CN) units on electron-accepting quinoxaline acceptors were designed and synthesized. To develop target polymers, thiophene-substituted benzodithiophene (BDT) units were selected as the primary electron-donating building blocks because of their advantages such as good electron-donating capability, high planarity, and less steric hindrance [19]. In addition, an electron-withdrawing chlorine (Cl) atom was introduced at the 4-position of the thiophene substituents on the BDT donor. This is because the insertion of Cl into BDT donor can induce positive effects on the photovoltaic performances of the resultant D-A type polymers [20, 21]. Subsequently, quinoxaline with two methoxy-substituted triphenylamine (methoxy-TPA) moieties on its 2,3-positions was adopted as the electron-accepting component. The two existing methoxy-TPA moieties can serve as additional electron donors in the vertical direction of the quinoxaline acceptor. Moreover, the strong electron-withdrawing F or CN moiety was selectively incorporated at the 5-position of the quinoxaline acceptor to analyze their effects on the photovoltaic properties of the polymers. Finally, the polymerization of the BDT donor with F- and CN-substituted quinoxaline acceptors, denoted as PBCl-MTQF and PBCl-MTQCN, respectively, can yield the desired polymers. By employing the well-known fused-ring-type small molecule Y6 as an *n*-type NFA [22], inverted-type devices with the structure of indium tin oxide (ITO)/SnO/polymer:Y6/MoO_3/Ag were fabricated. The power conversion efficiency (PCE) of the fluorinated PBCl-MTQF was 7.48%, whereas that of the CN-substituted PBCl-MTQCN was limited to 3.10%. These results clearly demonstrate the significant effect of the strong electron-withdrawing F and CN substituents on the photovoltaic properties of the corresponding two-dimensional (2D) quinoxaline-based polymers.

Results And Discussion

Synthesis and characterization of polymers

The preparation routes for the monomers and polymers are shown in Scheme 1, and their synthetic details and analytical results are described in the experimental section of the Electronic Supporting Information (ESI). First, the reaction of 1-iodo-4-methoxybenzene with aniline-afforded *N*,*N*-bis(4-methoxyphenyl)benzenamine (1) was performed. Second, *α*-diketone 1,2-bis(4-(bis(4-methoxyphenyl)amino)phenyl)ethane-1,2-dione (2) was prepared via the Friedel–Crafts reaction of 1 in the presence of oxalyl chloride [23]. Third, two reactions, i.e., zinc-mediated reduction and condensation, were performed on 4,7-dibromo[*c*][1, 2, 5]thiadiazole derivatives (3 and 4) to synthesize dibrominated quinoxaline monomers with strong electron-withdrawing F (5) and CN substituents (6). Finally, the polymerization of a chlorinated BDT donor (7) with 5 and 6 under the Stille coupling condition yielded the target D–A-type quinoxaline-based polymers, i.e., PBCl-MTQF and PBCl-MTQCN, respectively. In this synthetic strategy, a unique 2D polymeric architecture, in which the electron-donating BDT and methoxy-TPA groups are located in the horizontal and vertical directions of the electron-accepting quinoxaline unit, respectively, was achieved. The formation of the 2D structure not only strengthened the structural uniqueness of the target polymers, but also induced broad light absorption and reduced the bandgap through the facile electron transfer process in both directions. The molecular weights of the polymers were analyzed via gel permeation chromatography using *o*-dichlorobenzene as the eluent. The number-average molecular weight and polydispersity index of PBCl-MTQF and PBCl-MTQCN were 20.82 kDa and 2.48, and 26.23 kDa and 2.24, respectively. These polymers exhibited good solubility in various organic solvents such as chloroform, toluene, and chlorobenzene, owing to the existence of 2-ethylhexyl and methoxy side chains on BDT and quinoxaline units, respectively.

Optical and electrochemical properties

The optical properties of the polymers were analyzed using ultraviolet–visible (UV–Vis) spectroscopy. As shown in Figures 1a and 1b, all polymers exhibited two similar absorption peaks in both the chloroform solution and film on the glass substrate. The peak in the shorter wavelength region of 300–450 nm was associated with the π–π* transitions of the conjugated backbones, whereas that at longer wavelength regions of 450–650 nm originated from the formation of an ICT state between the donor and acceptor units in the polymer chains. The molar extinction coefficients (*ε*) in the ICT region of PBCl-MTQF and PBCl-MTQCN in chloroform solution were 6.12×10^4 and 6.50×10^4 M^{-1} cm^{-1}, respectively (Figure 1a). The maximum absorption peak of PBCl-MTQCN was red shifted by approximately 10 nm compared with that of PBCl-MTQF. The higher *ε* value of PBCl-MTQCN at longer wavelengths compared with that of PBCl-MTQF can be attributed to the stronger ICT formation caused by the availability of more electron-withdrawing CN units [24]. The electronic effects of the substituent can be correlated with the Hammett constant, and the values for F and CN at meta-positions were determined to be 0.34 and 0.56, respectively [25]. The two polymers exhibited good complementary light absorption spectra with an *n*-type Y6 acceptor in the film state (Figure 1b), which is beneficial for improving the photovoltaic properties of the devices. In addition, the optical bandgaps of PBCl-MTQF and PBCl-MTQCN calculated from the absorption edge in film state were 1.81 and 1.80 eV, respectively.

The electrochemical properties of the polymers were analyzed using cyclic voltammetry (CV) measurements with a ferrocene (Fc)/ferrocenium (Fc^+) external standard. The energy levels of the highest occupied molecular orbital (HOMO) and lowest unoccupied molecular orbital (LUMO) were determined from the onset oxidation and reduction potentials, respectively, in the CV curves (Figure 1c). The calculated HOMO/LUMO energy levels of PBCl-MTQF and PBCl-MTQCN were −5.06/−3.27 and −5.14/−3.38 eV, respectively. The higher electron-withdrawing capability of the CN unit compared with that of the F atom in the quinoxaline acceptor can induce a significant reduction in both the HOMO and LUMO energy levels of PBCl-MTQCN compared with those of PBCl-MTQF. In addition, the electrochemical bandgaps of PBCl-MTQF and PBCl-MTQCN estimated from the difference between their HOMO and LUMO energy levels were 1.79 and 1.76 eV, respectively. The electrochemical bandgap of the polymers exhibited the same trend as the optical bandgaps. The optical and electrochemical properties of the polymers are listed in Table 1. Based on the results, it was discovered that the replacement of the F atom with the CN moiety in the quinoxaline acceptor significantly affected the optical and electrochemical properties of the corresponding D–A-type polymers.

Table 1
Optical and electrochemical properties of the polymers.

Polymers	ε (M^{-1} cm^{-1})	E_{gap}^{opt} [a] (eV)	$\lambda_{max}^{solution}$ (nm)[b]	HOMO (eV)[c]	LUMO (eV)[d]	E_{gap}^{elec} (eV) [e]
PBCl-MTQF	6.16×10^4	1.81	366, 536	-5.06	-3.27	1.79
PBCl-MTQCN	6.50×10^4	1.80	370, 548	-5.14	-3.38	1.76

[a]Estimated from the absorption edge in the film state. [b]Maximum absorption wavelengths of polymers in chloroform solution. [c]Estimated from the oxidation onset potential. [d]Estimated from the reduction onset potential. [e]Calculated from the oxidation and reduction onset potentials in the CV curves.

Theoretical calculation

Density functional simulations using the Gaussian 09 program at the B3LYP/6-31G** level were performed to estimate the optimized geometries and frontier molecular orbitals of the polymers [26]. To reduce complicated computational calculations, 2-ethylhexyl chains on BDT donors and long polymer backbones were simplified to the shortest methyl group and small dimer unit, respectively. In the optimized geometries, the dihedral angles between the thiophene unit and quinoxaline acceptor in the polymer backbone changed significantly from 16.34° in PBCl-MTQF to 41.16° in PBCl-MTQCN (Figure 2). The increased steric hindrance induced by the substitution of the bulkier CN moiety instead of the F atom can readily generate more twisted conformation in PBCl-MTQCN. From the viewpoint of frontier molecular orbitals, similar characteristic features were observed in the two polymers. The HOMO wave functions of all the polymers were localized on the methoxy-TPA units, whereas their LUMO wave

functions were delocalized along the polymer backbones. However, the HOMO and LUMO energy levels of the polymers were altered significantly by the type of electron-withdrawing substituent on the quinoxaline acceptor. The simulated HOMO/LUMO energy levels of PBCl-MTQF and PBCl-MTQCN were −4.68/−2.38 eV and −4.74/−2.51 eV, respectively. Both the HOMO and LUMO energy levels of PBCl-MTQCN were more stable than those of PBCl-MTQF. As experimentally observed based on the HOMO/LUMO energy levels of the polymers using CV measurements, the theoretical HOMO/LUMO energy levels of the polymers reduced owing to the substitution of F atom with CN moiety.

Photovoltaic Properties

To investigate the effects of the CN and F substituents on the photovoltaic properties of the polymer, we introduced an inverted device configuration of ITO/SnO/polymer:Y6/MoO_3/Ag (Figure 3a). Because Y6 is one of the best non-fullerene acceptors for sufficient light absorption and efficient charge transport [7], we selected Y6 as an electron acceptor for device fabrication. As shown in Figure 3b, the HOMO and LUMO levels of both polymers agreed well with those of Y6 for cascade energy level alignment. For device optimization, various D:A ratios of the active layers of the devices were tested (Figure S1 and Table S1 in the ESI). The optimum devices comprising PBCl-MTQF and PBCl-MTQCN had D:A ratios of 1:1.5 and 1:1.0, respectively, in the presence of 1,8-diiodooctane as a processing additive. The current density–voltage (*J*– *V*) characteristics and the external quantum efficiency (EQE) of the optimized devices are shown in Figures 3c and 3d, respectively. The corresponding photovoltaic parameters are presented in Table 2. It was discovered that the device based on PBCl-MTQF exhibited a higher PCE of 7.48% with a short-circuit current density (J_{SC}) of 19.26 mA/cm^2, open-circuit voltage (V_{OC}) of 0.71 V, and fill factor (*FF*) of 0.54. By contrast, the device based on PBCl-MTQCN indicated lower values for their photovoltaic parameters (PCE, 3.10%; J_{SC}: 11.46 mA/cm^2, V_{OC}, 0.67; and *FF*, 0.39). In addition, the EQE curves of both devices encompassed broad wavelengths ranging from 350 to 950 nm (Figure 3d). The maximum EQE value of the device based on PBCl-MTQF was 67% higher than that of the device based on PBCl-MTQCN (44%). The calculated J_{SC} values from the EQE curves were consistent with those obtained from the *J*– *V* characteristics. These results demonstrate the significant dependence of the photovoltaic performance of D-A-type quinoxaline-based polymers on the type of electron-withdrawing substituent on the quinoxaline acceptor.

Table 2
Best photovoltaic parameters of PSCs. Values in parentheses represent average (of 10 devices) value of photovoltaic parameters for each device.

Polymer	Blend Ratio (Polymer:Y6)	J_{SC} (mA/cm^2)	J_{SC} (mA/cm^2)[a]	V_{OC} (V)	*FF*	*PCE* (%)
PBCl-MTQF	1:1.5	19.26	19.13	0.71	0.54	7.48 (7.21 ± 0.20)[b]
PBCl-MTQCN	1:1	11.46	11.12	0.67	0.39	3.10 (2.80 ± 0.31)[b]

[a]Calculated from EQE curves of the devices. [b]Values in parenthesis mean average PCE.

Charge recombination characteristics

To further evaluate the charge transport characteristics of the active blends in single-carrier devices, *J*–*V* characteristics of the electron- and hole-only devices were analyzed with a well-known space-charge-limited-current model [27]. The structures of the devices employed were ITO/SnO/active layer/LiF/Al and ITO/PEDOT:PSS/active layer/Au for the electron- and hole-only devices, respectively. The characteristic *J*–*V* curves of the single-carrier devices are shown in Figure S2 and Table S2 in the ESI. The electron (μ_e) and hole (μ_h) mobilities of the PBCl-MTQF:Y6 device were measured to be $1.8 \cdot 10^{-4}$ and $3.2 \cdot 10^{-4}$ cm^2 V^{-1} s^{-1}, whereas those of the PBCl-MTQCN:Y6 device were $1.2 \cdot 10^{-4}$ and $2.0 \cdot 10^{-4}$ cm^2 V^{-1} s^{-1}, respectively. The decreased charge transfer ability of the PBCl-MTQCN:Y6 device might have contributed to the lower J_{SC} values. Owing to the high μ_e and μ_h values of PBCl-MTQF:Y6, high values of J_{SC} and *FF* were observed, which might have promoted charge transfer in the device performance. To compare the charge recombination behaviors of the devices comprising PBCl-MTQF and PBCl-MTQCN, we measured the dependence of J_{SC} and V_{OC} on light intensity. Figures 4a and 4b show the J_{SC} and V_{OC} dependence curves as a function of light intensity, respectively. Based on the power-law relationship, the J_{SC} vs. light intensity (P_{light}) can be described as $J_{SC} \propto P_{light}^{\alpha}$, where α is the power-law factor and reflects the tendency of bimolecular recombination [28]. The α value of approximately unity in the log–log plot of J_{SC} vs. light intensity indicates weak bimolecular recombination under short-circuit conditions [29]. As shown in Figure 4a, the PBCl-MTQF and PBCl-MTQCN devices exhibited α values of 0.97 and 0.86, respectively. These results indicate the suppression of undesirable bimolecular recombination loss in the PBCl-MTQF device, whereas dominant bimolecular charge-carrier recombination loss was observed in the PBCl-MTQCN device during charge transfer.

The relationship between the V_{OC} of the devices and light intensity can be expressed as $V_{oc} = (nkT/q) \times \ln[\frac{J_{ph}}{J_o} + 1]$, where n is the ideality factor, k the Boltzmann constant, T the absolute temperature, and q the elementary charge. The slope from the V_{OC}–light intensity curve provides information regarding the trap-assisted recombination loss within the device [30, 31]. As shown in Figure 4b, the devices comprising PBCl-MTQF and PBCl-MTQCN exhibited n values of 1.08 kT/q and 1.91 $kT/$q, respectively. The PBCl-

MTQF device exhibited a lower *n* value, indicating reduced trap-assisted recombination during charge transfer. By contrast, the introduction of CN groups can significantly increase the population of trap-assisted recombination, thereby decreasing the charge mobility in the device. Weak bimolecular and trap-assisted recombination losses enable higher efficiencies in devices based on PBCl-MTQF.

To further evaluate the exciton dissociation and charge extraction properties, we analyzed the correlation between the photocurrent density (J_{ph}) and effective voltage (V_{eff}), where $J_{ph} = J_L$ (current density under illumination) – J_D (current density in dark) and $V_{eff} = V_0$ (voltage at J_{ph} = 0) - V_a (applied voltage) (Figure 4c). At V_{eff} >> 2.0 V, the saturated *Jsc* values of devices PBCl-MTQF and PBCl-MTQCN with Y6 were calculated to be 19.43 and 11.67 mA cm^{-2}, respectively (Figure 4c). Under the short-circuit conditions, the dissociation probability [*P(E,T)*] at the D/A interfaces was calculated to be 98.2% (PBCl-MTQF) and 94.6% (PBCl-MTQCN).[32] Additionally, the maximum charge collection efficiency of the devices with PBCl-MTQF and PBCl-MTQCN were 70.1% and 22.7%, respectively. The high J_{sc} and PCE values of the PBCl-MTQF device was due to the efficient exciton dissociation and charge collection efficiency. In general, the device comprising PBCl-MTQF exhibited better charge recombination and charge extraction properties compared with the device comprising PBCl-MTQCN.

Morphology of blended films

To analyze the surface morphology of the active layer, atomic force microscopy (AFM) measurements were performed in the tapping mode, and the resultant images are shown in Figure 5. The polymer:Y6 blend films based on different polymers showed distinct morphological differences. A homogeneous spherical morphology was observed for the blend film comprising PBCl-MTQF, whereas the film comprising PBCl-MTQCN exhibited an irregular granular morphology. Consequently, the blend film comprising PBCl-MTQF exhibited a relatively uniform film and contained bicontinuous interpenetrating networks, as compared with the film comprising PBCl-MTQCN. The larger domain size of the film comprising PBCl-MTQCN yielded a high root-mean-square (RMS) surface roughness of 5.4 nm, compared with that of the film comprising PBCl-MTQF (RMS value of 3.1 nm). The introduction of CN-groups in the polymer chain resulted in the formation of larger DA domains, which hindered efficient exciton dissociation and charge transport.

To investigate the molecular orientation and crystallinity of the neat and blended films, grazing incidence X-ray scattering (GIWAXS) measurements were performed. Their GIWAXS patterns and corresponding line-cut profiles are shown in Figure 6. The corresponding GIWAXS parameters are listed in Table S3 in the ESI. The neat PBCl-MTQF film exhibited an extremely weak π–π stacking (010) peak at 1.54 $Å^{-1}$ in the out-of-plane (OOP) direction and multiple lamellar packing (h00) diffraction peaks in the in-plane (IP) direction (Figure 6a). This suggests that the PBCl-MTQF film exhibited different packing modes with moderate crystalline features, indicating a moderate face-on orientation in favor of charge transport. By contrast, the neat PBCl-MTQCN film exhibited a relatively clear π–π stacking (010) peak at 1.51 $Å^{-1}$ and multiple lamellar packing (h00) peaks in the OOP and IP directions, respectively (Figure 6b), indicating the

stronger crystalline properties of PBCl-MTQCN compared with that of PBCl-MTQF in the pristine polymer state. Moreover, pristine PBCl-MTQF and PBCl-MTQCN films showed different crystal coherence length (CCL) of 6.25 and 7.67 Å, respectively, suggesting the stronger crystallinity of PBCl-MTQCN. The neat film of Y6 exhibited a strong π−π stacking diffraction peak in the OOP direction at 1.72 $Å^{-1}$ (d = 3.65 $Å^{-1}$), and two other diffraction peaks at q = 0.27 and 0.415 $Å^{-1}$ in the IP direction (Figure S3 in ESI). This suggests the coexistence of two different ordered structures in Y6.

The GIWAXS analysis of the blended films revealed that both blend films exhibited a lamellar diffraction peak (100) along the IP direction and a clear π−π stacking diffraction peak (010) in the OOP direction (Figures 6c and 6d). The GIWAXS pattern of the PBCl-MTQF:Y6 blend film showed a dominant diffraction peak for Y6 (Figure S3 in ESI). These results agreed relatively well with those of the pristine PBCl-MTQF film as compared with those of PBCl-MTQCN. Hence, a more homogeneous mixing between PBCl-MTQF and Y6 can be expected in the blend film, which is consistent with the AFM results (Figure 5a). The CCL values of the pristine films confirmed the strong internal π−π stacking in PBCl-MTQCN compared with that of PBCl-MTQF, which indicates a stronger intramolecular interaction in PBCl-MTQCN. By contrast, the blends of PBCl-MTQF:Y6 showed an enhanced crystalline phase with coherence to the pristine Y6 diffraction peaks; this yielded a more preferable face-on molecular orientation packing, which is advantageous for charge transport.

Conclusion

Two-dimensional quinoxaline-based D−A type polymers of PBCl-MTQF and PBCl-MTQCN, in which the strong electron-withdrawing substituents of F and CN units were selectively incorporated, respectively, were synthesized via the Stille coupling reaction to investigate their effects on the photovoltaic properties of the polymers. Owing to the higher electron-withdrawing capability of the CN moiety compared with that of the F atom, PBCl-MTQCN exhibited not only a higher ε value in the ICT region, but also a lower HOMO energy level compared with PBCl-MTQF. Under these conditions, the concomitant enhancement in the *Jsc*, *Voc*, and PCE of the PBCl-MTQCN-based device can be anticipated. However, a higher PCE of 7.45% was achieved from the PBCl-MTQF-based device, which exhibited a *Jsc* of 19.43 mA/cm^2, *Voc* of 0.71 V, and FF of 0.54. The PCE of the PBCl-MTQCN-based device was restricted to 3.10%, with a *Jsc* of 11.46 mA/cm^2, *Voc* of 0.67 V, and FF of 0.39. Hence, it was clear that the *Jsc*, *Voc*, and PCE of the PBCl-MTQCN-based device were inferior to those of the PBCl-MTQCN-based device. The significant reduction in the *Jsc* and FF of the PBCl-MTQCN-based device was attributable to the unfavorable aggregation-induced charge recombination and charge transport kinetics. Owing to the high aggregation behavior of PBCl-MTQCN, as revealed via AFM, a significant amount of undesirable bimolecular recombination loss was observed during charge transport. Therefore, the incorporation of electron-withdrawing substituents on the quinoxaline-based polymers must be controlled well because their photovoltaic properties are affected significantly by the type of existing substituents. This study provides valuable information regarding the structure−property relationships of D−A-type quinoxaline-based polymers for photovoltaic applications.

Declarations

Acknowledgement

First two authors contributed equally to this work. This research was supported by Basic Science Researches through the National Research Foundation (NRF) of Republic of Korea under program number (NRF-2021R1A2C1003755 and NRF-2020H1D3A1A04080437). This work also funded by NRF of Korea (NRF-2020R1A4A1019183) under the program of Basic Research Laboratory (BRL).

References

1. Lee, J. *et al.* Slot-Die and Roll-to-Roll Processed Single Junction Organic Photovoltaic Cells with the Highest Efficiency. *Advanced Energy Materials*, **9**, 1–9 (2019).
2. Lu, L. *et al.* Recent Advances in Bulk Heterojunction Polymer Solar Cells. *Chem. Rev*, **115**, 12666–12731 (2015).
3. Li, G., Zhu, R. & Yang, Y. Polymer solar cells. *Nature Photonics*, **6**, 153–161 (2012).
4. Dennler, G., Scharber, M. C. & Brabec, C. J. Polymer-Fullerene Bulk-Heterojunction Solar Cells. *Adv. Mater*, **21**, 1323–1338 (2009).
5. Yan, C. *et al.* Non-fullerene acceptors for organic solar cells. *Nature Reviews Materials*, **3**, 1–19 (2018).
6. Sun, H., Chen, F. & Chen, Z. K. Recent progress on non-fullerene acceptors for organic photovoltaics. *Mater. Today*, **24**, 94–118 (2019).
7. Armin, A. *et al.* A History and Perspective of Non-Fullerene Electron Acceptors for Organic Solar Cells. *Advanced Energy Materials*, **11**, 1–42 (2021).
8. Liu, Q. *et al.* 18% Efficiency organic solar cells. *Science Bulletin*, **65**, 272–275 (2020).
9. An, C., Zheng, Z. & Hou, J. Recent progress in wide bandgap conjugated polymer donors for high-performance nonfullerene organic photovoltaics. *Chem. Commun*, **56**, 4750–4760 (2020).
10. Liu, M., Gao, Y., Zhang, Y., Liu, Z. & Zhao, L. Quinoxaline-based conjugated polymers for polymer solar cells. *Polym. Chem*, **8**, 4613–4636 (2017).
11. Gao, L. *et al.* High-Efficiency Nonfullerene Polymer Solar Cells with Medium Bandgap Polymer Donor and Narrow Bandgap Organic Semiconductor Acceptor. *Adv. Mater*, **28**, 8288–8295 (2016).
12. Xu, X. P., Li, Y., Luo, M. M. & Peng, Q. Recent progress towards fluorinated copolymers for efficient photovoltaic applications. *Chin. Chem. Lett*, **27**, 1241–1249 (2016).
13. Sun, H. *et al.* A monothiophene unit incorporating both fluoro and ester substitution enabling high-performance donor polymers for non-fullerene solar cells with 16.4% efficiency. *Energy and Environmental Science*, **12**, 3328–3337 (2019).
14. Price, S. C., Stuart, A. C., Yang, L., Zhou, H. & You, W. Fluorine substituted conjugated polymer of medium band gap yields 7% efficiency in polymer-fullerene solar cells. *Journal of the American*

Chemical Society, **133**, 4625–4631 (2011).

15. Zhang, Y., Zhou, P., Wang, J., Zhan, X. & Chen, X. Designing a thiophene-fused quinoxaline unit to build D–A copolymers for non-fullerene organic solar cells. *Dyes and Pigments*, **174**, 108022 (2020).
16. Yang, M. H. *et al.* Roll-to-roll compatible quinoxaline-based polymers toward high performance polymer solar cells. *Journal of Materials Chemistry A*, **8**, 25208–25216 (2020).
17. Yang, J. *et al.* Quinoxaline-Based Wide Band Gap Polymers for Efficient Nonfullerene Organic Solar Cells with Large Open-Circuit Voltages. *ACS Applied Materials and Interfaces*, **10**, 23235–23246 (2018).
18. Handoko, S. L. *et al.* Synthesis of quinoxaline-based polymers with multiple electron-withdrawing groups for polymer solar cells. *Journal of Industrial and Engineering Chemistry*, **73**, 192–197 (2019).
19. Yao, H. *et al.* Molecular design of benzodithiophene-based organic photovoltaic materials. *Chem. Rev*, **116**, 7397–7457 (2016).
20. Zhang, S., Qin, Y., Zhu, J. & Hou, J. Over 14% Efficiency in Polymer Solar Cells Enabled by a Chlorinated Polymer Donor. *Adv. Mater*, **30**, 1–7 (2018).
21. Lenaerts, R. *et al.* The effect of halogenation on PBDTT-TQxT based non-fullerene polymer solar cells – Chlorination vs fluorination. *Dyes and Pigments*, **181**, 108577 (2020).
22. Yuan, J. *et al.* Single-Junction Organic Solar Cell with over 15% Efficiency Using Fused-Ring Acceptor with Electron-Deficient Core. *Joule*, **3**, 1140–1151 (2019).
23. Chen, W., Tan, S. Y., Zhao, Y. & Zhang, Q. A concise method to prepare novel fused heteroaromatic diones through double Friedel-Crafts acylation. *Organic Chemistry Frontiers*, **1**, 391–394 (2014).
24. Sagita, C. P. *et al.* Enhanced photovoltaic performance of quinoxaline-based donor-acceptor type polymers with monocyano substituent. *Journal of Power Sources*, **491**, 229588 (2021).
25. Hansch, C., Leo, A. & Taft, R. W. A Survey of Hammett Substituent Constants and Resonance and Field Parameters. *Chem. Rev*, **91**, 165–195 (1991).
26. Chen, S. *et al.* High-performance polymer solar cells with efficiency over 18% enabled by asymmetric side chain engineering of non-fullerene acceptors. *Science China Chemistry*, **64**, 1192–1199 (2021).
27. Blakesley, J. C. *et al.* Towards reliable charge-mobility benchmark measurements for organic semiconductors. *Org. Electron*, **15**, 1263–1272 (2014).
28. Pang, S. *et al.* Nonfused Nonfullerene Acceptors with an A-D-A'-D-A Framework and a Benzothiadiazole Core for High-Performance Organic Solar Cells. *ACS Applied Materials and Interfaces*, **12**, 16531–16540 (2020).
29. Koster, L. J. A., Mihailetchi, V. D., Ramaker, R. & Blom, P. W. M. Light intensity dependence of open-circuit voltage of polymer:fullerene solar cells. *Appl. Phys. Lett*, **86**, 1–3 (2005).
30. Xiao, Z., Geng, X., He, D., Jia, X. & Ding, L. Development of isomer-free fullerene bisadducts for efficient polymer solar cells. *Energy and Environmental Science*, **9**, 2114–2121 (2016).
31. Mandoc, M. M., Kooistra, F. B., Hummelen, J. C., De Boer, B. & Blom, P. W. M. Effect of traps on the performance of bulk heterojunction organic solar cells. *Appl. Phys. Lett*, **91**, 2005–2008 (2007).

32. Mihailetchi, V. D., Xie, H., De Boer, B., Koster, L. J. A. & Blom, P. W. M. Charge transport and photocurrent generation in poly(3-hexylthiophene): Methanofullerene bulk-heterojunction solar cells. *Adv. Funct. Mater*, **16**, 699–708 (2006).

Scheme 1

Scheme 1 in the Supplementary Files.

Supplementary Files

"Figure S1 and Table S1 are not available with this version."

Figures

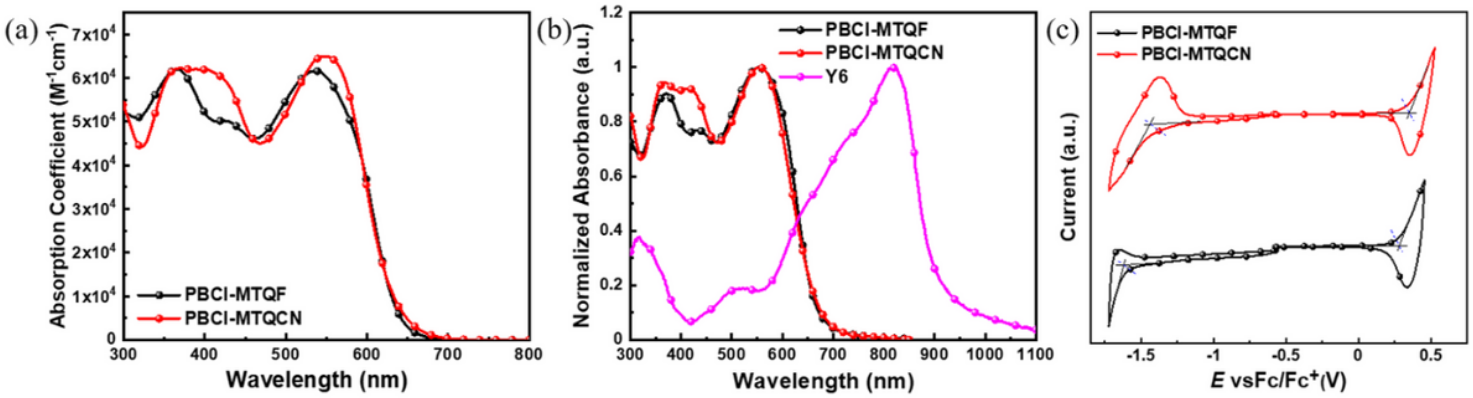

Figure 1

(a) UV–Vis spectra of (a) polymers in chloroform solution and (b) polymers and Y6 in film on glass substrate. (c) CV curves of polymers.

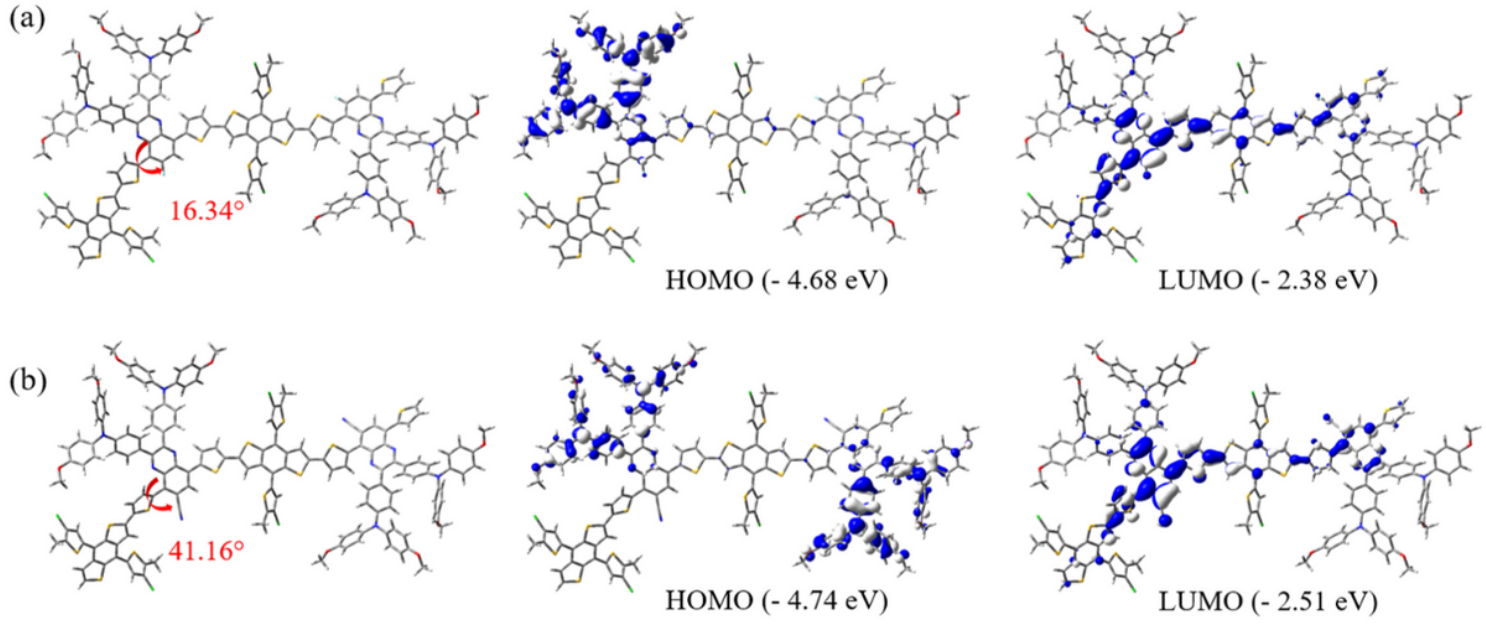

Figure 2

Optimized geometries and frontier molecular orbitals of two-repeating unit calculated HOMO/LUMO energy levels at B3LYP/6-31G** level for (a) PBCl-MTQF and (b) PBCl-MTQCN.

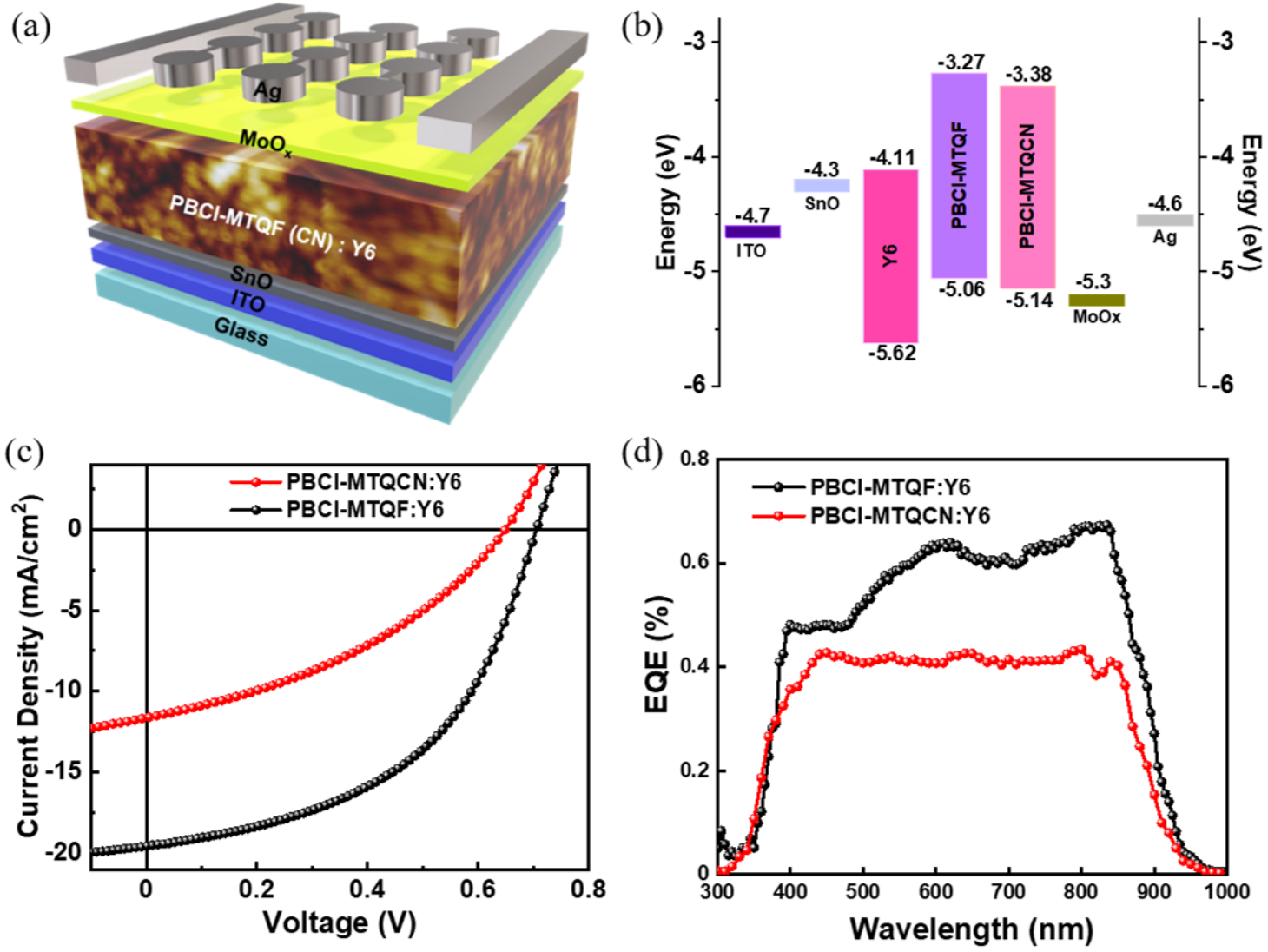

Figure 3

(a) Structure, (b) energy band diagram, (c) J–V curves and (b) EQE curves of inverted-type device based on PBCl-MTQF and PBCl-MTQCN as polymeric donor.

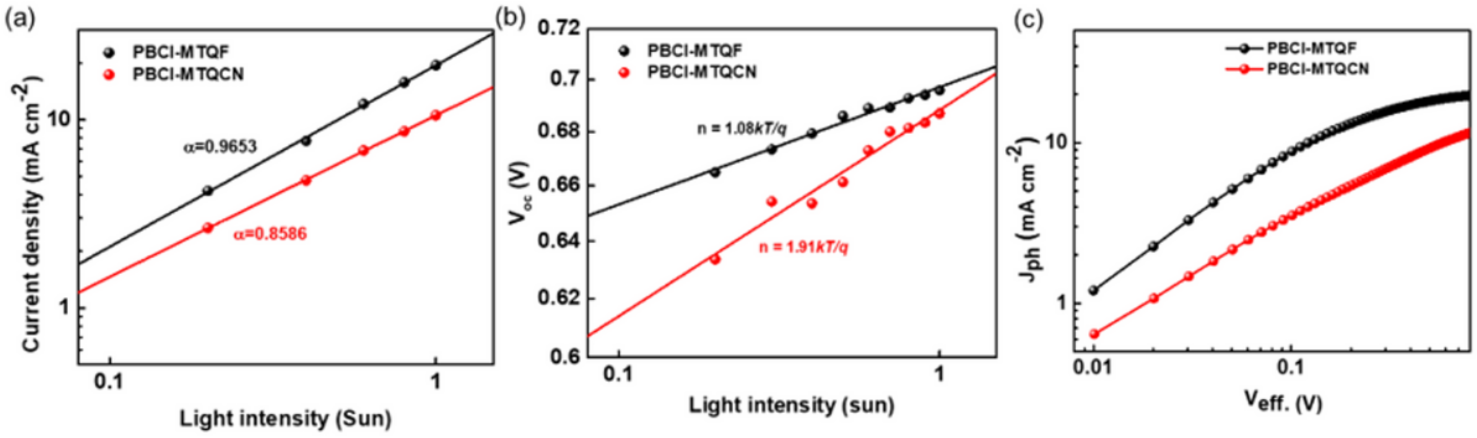

Figure 4

(a) Jsc vs. light intensity plots and (b) Voc vs. light intensity plots of devices. (c) Jph–Veff curves of polymers.

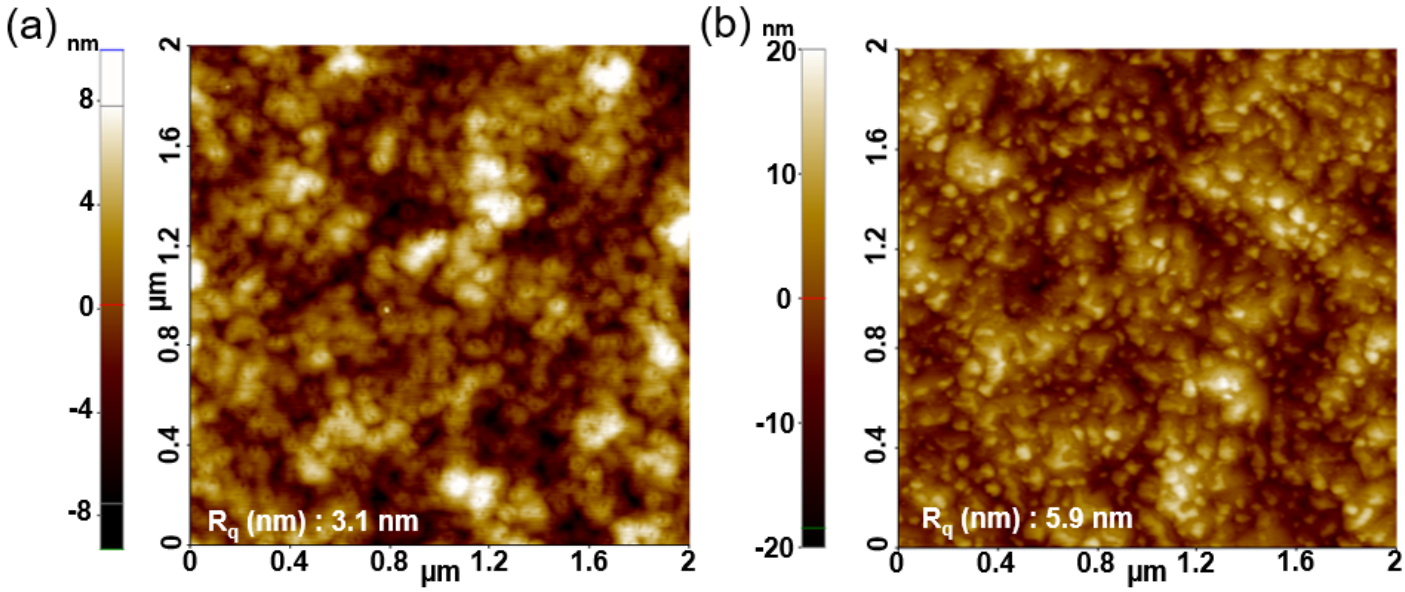

Figure 5

Tapping-mode AFM images of blend films of (a) PBCl-MTQF and (b) PBCl-MTQCN with Y6.

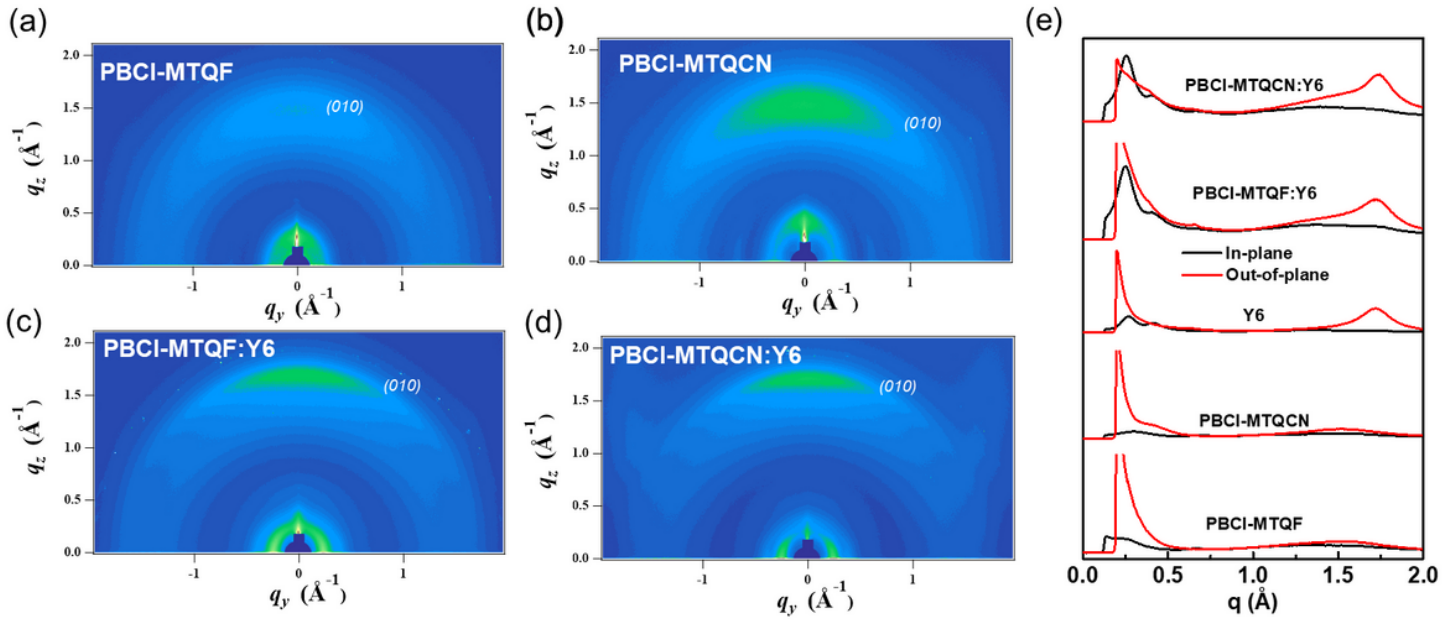

Figure 6

GIWAXS patterns of (a,b) neat films and (c,d) blend films of PBCl-MTQF and PBCl-MTQCN. (e) Line-cut profiles of neat and blend films (red line: out-of-plane; black line: in-plane).

Supplementary Files

This is a list of supplementary files associated with this preprint. Click to download.

- floatimage1.png
- floatimage2.png